Available online at www.sciencedirect.com
ScienceDirect
Estuarine, Coastal and Shelf Science 69 (2006) 403–413
ESTUARINE COASTAL AND SHELF SCIENCE
www.elsevier.com/locate/ecss

Effects of crab–halophytic plant interactions on creek growth in a S.W. Atlantic salt marsh: A Cellular Automata model

Darío R. Minkoff [a,*], Mauricio Escapa [a,b], Félix E. Ferramola [c], Silvio D. Maraschín [a], Jorge O. Pierini [a,d,e], Gerardo M.E. Perillo [a,f], Claudio Delrieux [c]

[a] *Instituto Argentino de Oceanografía, CC 804, 8000 Bahía Blanca, Argentina*
[b] *Depto. de Biología (FCEyN), Universidad Nacional de Mar del Plata, CC 573 Correo Central (7600), Mar del Plata, Argentina*
[c] *Depto de Ingeniería Eléctrica y Computadoras, Universidad Nacional del Sur, Avenida Alem 1253, Bahía Blanca, Argentina*
[d] *Depto. de Física, Universidad Nacional del Sur, Alem 1253, 8000 Bahía Blanca, Argentina*
[e] *Comisión de Investigaciones Científicas de la provincia de Buenos Aires, Argentina*
[f] *Depto. de Geología, Universidad Nacional del Sur, San Juan 670, 8000 Bahía Blanca, Argentina*

Received 7 April 2006; accepted 2 May 2006
Available online 3 July 2006

Abstract

The Bahía Blanca Estuary (38° 50′ S, and 62° 30′ W) presents salt marshes where interactions between the local flora (*Sarcocornia perennis*) and fauna (*Chasmagnathus granulatus*) generate some kind of salt pans that alter the normal water circulation and condition its flow and course towards tidal creeks. The crab–vegetation dynamics in the salt marsh presents variations that cannot be quantified in a reasonable period of time. The interaction between *S. perennis* plant and *C. granulatus* crab is based on simple laws, but its result is a complex biological mechanism that causes an erosive process on the salt marsh and favors the formation of tidal creeks. To study it, a Cellular Automata model is proposed, based on the laws deduced from the observation of these phenomena in the field, and then verified with measurable data within macroscale time units. Therefore, the objective of this article is to model how the interaction between *C. granulatus* and *S. perennis* modifies the landscape of the salt marsh and influences the path of tidal creeks. The model copies the basic laws that rule the problem based on purely biological factors.

The Cellular Automata model proved capable of reproducing the effects of the interaction between plants and crabs in the salt marsh. A study of the water drainage of the basins showed that this interaction does indeed modify the development of tidal creeks. Model dynamics would likewise follow different laws, which would provide a different formula for the probability of patch dilation. The patch shape can be obtained changing the pattern that dilates.

Keywords: Cellular Automata; tidal creek; salt pans; digital terrain model; Bahia Blanca Estuary; Argentina

1. Introduction

Salt marshes and tidal flats are typical coastal environments which normally develop in protected regions where tidal amplitude is important and where there is high sediment input. They are characterized by a relatively smooth topography, differentiated by the presence or absence of halophytic plants, exposed to oceanographic and atmospheric activities which give rise to fluctuations on the tidal wave propagation over the flats. At the same time, the continuous effect of tide and rain favors the genesis and development of salt pans and tidal creeks.

The two principal physiographic features in salt marshes are salt pans and tidal creeks (Chapman, 1960). Tidal creeks usually originate in tidal flats and they are inherited by the salt marshes in their process of colonization (Frey and Basan, 1985). The formation of tidal creeks is an erosive process that transfers tidal flats and salt marshes material to the embayment and in turn to the adjacent shelf. Furthermore, tidal creeks play

* Corresponding author.
E-mail address: dminkoff@criba.edu.ar (D.R. Minkoff).

0272-7714/$ - see front matter © 2006 Elsevier Ltd. All rights reserved.
doi:10.1016/j.ecss.2006.05.008

an important role in the hydrodynamics of tidal salt marshes by increasing drainage and flooding in their zone of hydrologic influence (Pestrong, 1965; Pethick, 1980; Marani et al., 2002).

In tidal flats, the development and evolution of the creeks is influenced by geologic, topographic and physical factors. However, in salt marshes a strong biological control must be added (Pestrong, 1972; Garofalo, 1980). The presence of vegetation on the channel banks influences their lateral migration. In turn the channels tend to be more sinuous with marked meandering than in more deserted zones of vegetation (Pestrong, 1972).

The Bahía Blanca Estuary (38° 50′ S and 62° 30′ W; Fig. 1) presents salt marshes where interactions between the local flora and fauna generate some kind of salt pans that alter the normal water circulation and condition its flow-path (Perillo and Iribarne, 2003a,b). This estuary has a total surface of 2300 km^2, of which about 410 km^2 correspond to islands and 1150 km^2 to the intertidal sector (Piccolo and Perillo, 1999). It is a mesotidal system with very little fluvial input covered by extensive tidal flats with predominance of low salt marshes, although a few mean and high marshes are observed.

The particular area where this study was developed corresponds to one of the few high marshes with an area of about 4.5 km^2 (Fig. 1) which is covered by the tides an average of 40 times a year and whose tidal amplitude reaches 0.6 m above the salt marsh. Waves rarely affect this zone because of the effect of vegetation and its protected placement.

In the SW Atlantic Ocean bays and estuaries, the tidal flats and salt marshes are dominated by the burrowing crab *Chasmagnathus granulatus* (Iribarne et al., 1997; Bortolus and Iribarne, 1999; Botto and Iribarne, 1999, 2000). This species lives in tidal flats and marshes vegetated by the halophytic plants of the genus *Spartina* and *Sarcocornia* (Spivak et al., 1994; Iribarne et al., 1997; Bortolus and Iribarne, 1999). The salt marsh under study is dominated by *Sarcocornia perennis*. This is a pioneer plant that dominates the marsh in the first successional stages; and grows forming circular clones (Perillo and Iribarne, 2003b). The circular or even ellipsoidal patches can reach from 0.30 to 10 m in diameter. Once the clones are established in the marsh, they could facilitate the activity of the burrowing crab *C. granulatus* which starts to dig its burrows below the plant canopies (Bortolus and Iribarne, 1999; Perillo and Iribarne, 2003b).

The bioturbation effects (feeding and burrowing activities) of crabs under the plants could generate changes in the sediment structure which affect plant growth. The primary patches start to sink and becomes slightly depressed due to the remotion of sediment by crabs and groundwater erosion. Thus, the central individuals of *Sarcocornia perennis* die due to sediment structure loss and inundation. As a consequence, a depressed ring is formed (called ‘‘ring salt pan’’), which continues growing outwards enclosing a population of crabs which in turn continues displacing the inner ring (Perillo and Iribarne, 2003a,b). In a more advanced state of growth, the rings will reach a diameter of 10 m being up to 1.5 m wide. Eventually in the proximity of another ring, they may join forming ‘‘8-like’’ figures or still more complex ones (called patch salt pan).

When there are isolated patches (ring salt pan structure) or several integrated patches (patch salt pan structure) near the arm of a creek, they behave like a concentrator of water when the tide ebbs or after rainfall, through which all the water is discharged to the creek. Because these pans are composed by a softer material with a high density of burrows (up 50 to per square meter) (Perillo and Iribarne, 2003b) they are easily eroded and become a new tributary of the creek where they drain. In all the salt marsh those pattern of ring salt pans and patch salt pans are associated with the formation of new creek tributaries.

These patch salt pans drain for a period of up to 2 h after the tide has retreated depending on their size. The erosive effect of water flow on the salt marsh is not as significant as when it

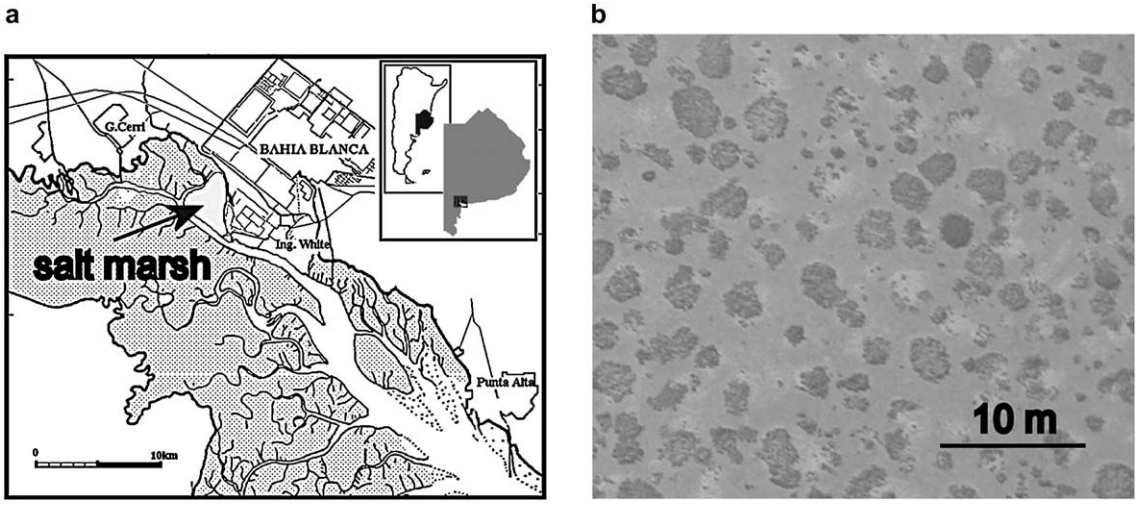

Fig. 1. (a) Bahía Blanca Estuary. The salt marsh under study is highlighted. (b) Air photography of the salt marsh where the distribution of patches of *Sarcocornia perennis* plants can be observed.

arrives at the creek where all the flow is concentrated in a smaller area, generating truly important currents (up to 10–20 cm s^{-1}). The water drains mainly among the creek heads forming small waterfalls and by groundwater flow between the crab burrows next to the heads. The result is that the creek head retreats by means of different erosive mechanisms, namely headward erosion and sediment slumping with rates of growth between 4 and 50 cm $month^{-1}$, respectively.

The crab–vegetation dynamics in the salt marsh presents variations that cannot be quantified in a reasonable period of time. To study it, a conceptual model is proposed based on the laws deduced from observation of these phenomena in the field, and then verified with measurable data within macroscale time units (Perillo and Codignotto, 1989). The model is used to simulate marsh topography and the effects of the crab–vegetation interaction.

The interaction between the *Sarcocornia perennis* plant and the *Chasmagnathus granulatus* crab is based on simple laws, but it results in a complex biological mechanism that causes an erosive process on the salt marsh and favors the formation of tidal creeks. These types of processes based on simple laws have been accurately modeled with good precision by Cellular Automata models (Dunkerley, 1997; Matsinos and Troumbis, 2002; Aassine and El Jai, 2002; Bandini and Pavesi, 2002). It is particularly desirable to recreate the observed and measured laws in order to obtain an automatic way of reproducing the biological disturbances in the field and to analyze their effect on the generation of tidal creeks on the basis of the resulting digital terrain model (DTM).

Most models to generate DTMs proposed initially were based on purely mathematical criteria, both for topography generation with all the mathematical variants, and river and channel path (Fournier et al., 1982; Voss, 1985; Miller, 1986; Mastin et al., 1987; Kelley et al., 1988). Others, however, apply basic physical equations on the DTM, but they are purely conceptual and generally applied to landscape and photorealism activities (Miller, 1986; Muagrave et al., 1989). Later on, models incorporated more complex physical equations attempting to simulate the evolution of the land morphology under hydraulic conditions (Howard et al., 1994; Smith et al., 1997; Fagherazzi et al., 1999; Rinaldo et al., 1999a,b; Wei luo, 2001; D'Ambrosio et al., 2001; El Yacoubi et al., 2003).

Therefore, the objective of this article is to model how the interaction between *Chasmagnathus granulatus* and *Sarcocornia perennis* modifies the landscape of the salt marsh and influences the path of tidal creeks. The model copies the basic laws that rule the problem based on purely biological factors. Hence the problem has been subdivided into three differentiated topics each associated with a distinct methodology.

2. Methods

2.1. Model

The first phase is the generation of a DTM representing the marsh surface without the disturbances proper of the problem, namely the plants and crabs. A midpoint displacement algorithm with random additions in two dimensions adapted to the typical topography of the salt marshes is used. The second phase is to reproduce the landscape that generates the vegetative dynamics in the marsh together with the bioturbating effect of the crabs employing a Cellular Automata model. The basic laws of the problem are deduced from field measurements. Model results are verified with a second field data set.

Then, the final topography is a linear combination of results of the first and second phase of the problem. The topography is further analyzed to establish trapping conditions for the water when the tide ebbs or after rainfall. Finally, tidal channel evolution in the original terrain was contrasted with the terrain modified by biological factors.

2.2. Generation of undisturbed topography

The generation of the digital terrain model was based on the midpoint displacement algorithm with random additions in two dimensions, due to its ample acceptance and diffusion (Fournier et al., 1982; Mandelbrot, 1982). Many modifications of this algorithm can be found (Saupe, 1988), but the original introduced by Fournier et al., 1982 was employed here. This algorithm is based on purely mathematical principles and carries out a recursive process from the external edges of the grid inward that composes the land to model. In each point of the grid the assigned height depends on the height of the neighbouring points plus a random addition.

The fractal dimension of the DTM is 3-H, where H is the Hurst coefficient (Fournier et al., 1982; Mandelbrot, 1982). In this work, we adopted a Hurst coefficient equal to 0.8. In order to adapt the DTM to the characteristics of the salt marsh a lowpass filter was applied. The filter consists in averaging each point of the grid with a square subgrid of the original matrix of 13 cells to each side.

2.3. Evolution of the biological factors

Basically, Cellular Automata (CA) models are idealizations of real systems, applied in a dimension lattice, where the space and time are discrete variables. The laws that they represent are simple, can be deterministic or stochastic, and are applied simultaneously to all points of the grid. Definitions of CA are given by Wolfram (1984, 1994) and Sipper (1997) and a complete description can be found in Worsch (1999). Formally, they can be summarized by considering CA as a set of rules (A):

$$A = (L, S, N, f)$$

where L is a grid of d dimensions with cells c depending on the shape of the grid, S is the finite set of values that a cell can take, $N(c)$ is the neighbourhood of cells that interact with c, and f is the transition function that defines the dynamics of the CA. Thus the state:

$$s_{t+1} = f(s_t(N(c))) \quad (1)$$

That is, at any point of the grid, the state of the following step depends on the application of the transition function in the neighbourhood that interacts with it in the present step. In addition, initial and boundary conditions must be established for each problem.

The bidimensional CA model proposed is based on the bidimensional neighbourhood scheme of Moore (El Yacoubi et al., 2003) with a 5 cm resolution. The transfer functions are deduced by the rate of growth of the external and internal diameter of the rings, the internal vs external diameter relation and the accretion of the salt pan vs the external diameter. To simplify the problem, we suppose that the diameters correspond to circles with area equal to that of the patches. The initial condition is a random and uniform distribution of plant seeds. The distribution of external and internal diameters, the relation between the internal and external diameters and a power law between the area and perimeter of plant patches obtained from an aerial photography are controlling parameters for the model.

2.4. Cellular Automata model construction

As a first step in the model application, the external ring growth is studied by applying a transfer function where each cell that represents a portion of the plant (Fig. 2a) is transformed into a cell array (Fig. 2b) with a given probability distribution as the model iterates. This operation is known as dilation (González and Woods, 1992; Haralick and Shapiro, 1992) but it is conditioned to the probability distribution. The shape of the resulting array represents a circle formed by a small number of cells. The probability distribution may or may not be constant and must satisfy the law of real plant growth according to the external diameter, which was found to follow a law of percentage growth (Fig. 3a) that is well represented by a reciprocal function of the external diameter $D_{t\,\mathrm{e}}$ (in m) of the type measured at time t:

$$\mathrm{Ce}\% = \alpha + \frac{\beta}{D_{t\,\mathrm{e}}} \tag{2}$$

where Ce% is the expected percentage growth for the sampling period. The periods between samplings were 30 ± 10 days. In this case, the function obtained applying Eq. (2) to the data of Fig. 4a results (ANOVA $F_{1,98} = 608.72$, $p < 0.01$, Zar, 1999):

$$\mathrm{Ce}\% = -2.6391 + \frac{20.1662}{D_{t\,\mathrm{e}}} \tag{3}$$

This percent growth is:

$$\mathrm{Ce}\% = \frac{D_{t\,\mathrm{e}+1} - D_{t\,\mathrm{e}}}{D_{t\,\mathrm{e}+1}} \tag{4}$$

where $D_{t\,\mathrm{e}+1}$ is the external diameter measured after a given period of time.

Since the transfer function is probabilistic, a series of simulations of plant growth employing 20 plants for the set of probabilities (0.01, 0.02, 0.03, 0.04, 0.05, 0.1, 0.15,…,0.95) and 35 iterations were made. The results indicate that the area of the patch follows a different parabolic law for each probability as a function of the number of iterations (Fig. 4a), whereas the diameter follows a linear law for each probability, also as a function of the number of iterations (Fig. 4b) meaning that:

$$\frac{D_{t\,\mathrm{e}+1} - D_{t\,\mathrm{e}}}{\Delta I} = \alpha \tag{5}$$

where ΔI is the number of iterations to pass from $D_{t\,\mathrm{e}}$ to $D_{t\,\mathrm{e}+1}$ and α is a constant corresponding to the slope of a straight line. Regrouping Eq. (5) we obtain:

$$\frac{D_{t\,\mathrm{e}+1} - D_{t\,\mathrm{e}}}{D_{t\,\mathrm{e}+1}} = \frac{\alpha \Delta I}{D_{t\,\mathrm{e}+1}} \tag{6}$$

We assumed that ΔI is constant with unitary value, implying that one iteration of the model is equivalent to 30 days of patch growth. Being α and ΔI are constants, the probability for each percentage growth is a reciprocal of the diameter. Thus, curves of percentage growth were simulated according to the external diameter for different probabilities (Fig. 4c). These curves are also well represented by reciprocal functions of the type:

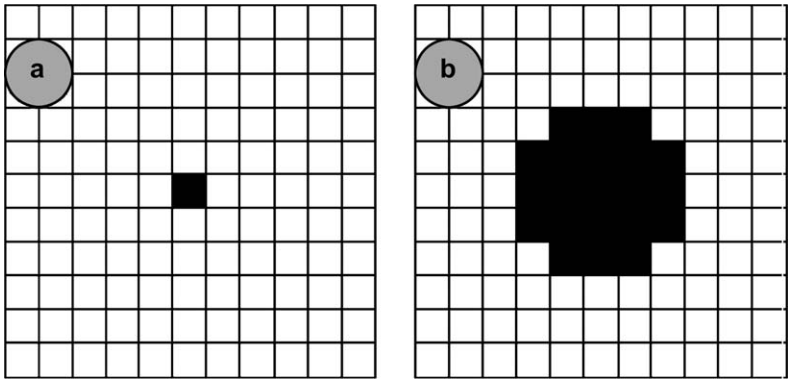

Fig. 2. Array by which a cell (a) can be dilated by an arrangement of cells (b).

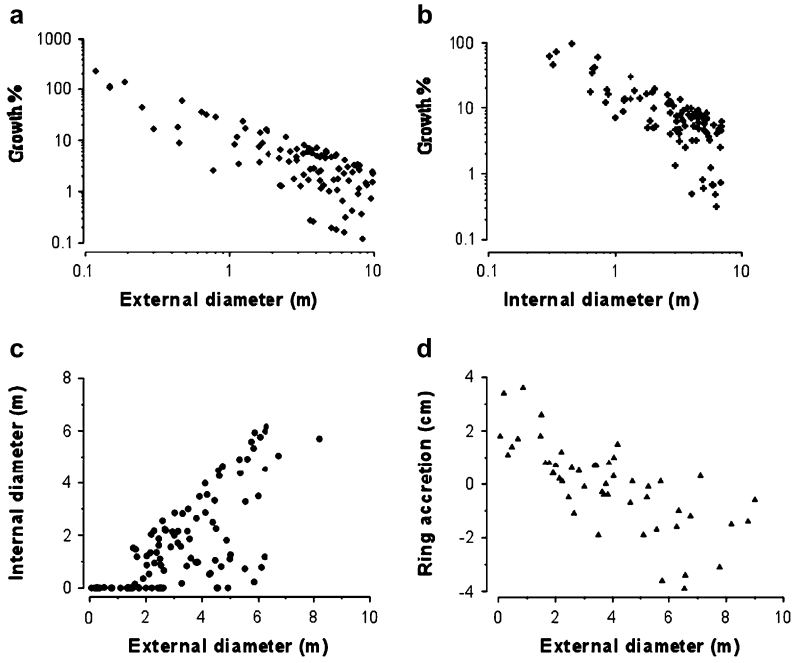

Fig. 3. Measured variables in the salt marsh with which functions of transition the Cellular Automata model was calculated. (a) Percentage growth of the external ring vs the external diameter of the *Sarcocornia perennis* ring for a sampling period, (b) percentage growth of the internal ring vs the internal diameter of the *S. perennis* ring for a sampling period, (c) relation between the internal diameter vs the external diameter of *S. perennis* rings and (d) accretion of the plant patch vs the external diameter of *S. perennis* rings.

$$D_{t\,\mathrm{e}+1} = a_{p_i} + \frac{b_{p_i}}{D_{t\,\mathrm{e}}} \tag{7}$$

where a_{p_i} and b_{p_i} are coefficients for the different probabilities p_i (Table 1).

The points through which the resulting curve of variable probabilities would have to pass are those where the curves of percentage growth for different probabilities cross the curve of real percentage growth. Equalling and clearing Eqs. (2) and (7) the diameters can be determined at the points where the curves cross (Table 1):

$$D_{t\,\mathrm{e}} = \frac{\beta - b_{p_i}}{a_{p_i} - \alpha} \tag{8}$$

Finally, we find that this relation of probabilities (Table 1, row 1) vs diameters (Table 1, row 7) is very well fitted by an asymptotic exponential curve (ANOVA $F_{1,16} = 3012.08$, $p < 0.01$, Zar, 1999):

$$\mathrm{Pr\_}D_{t\,\mathrm{e}} = 0.005427 + 0.6623\mathrm{e}^{\frac{-D_{t\,\mathrm{e}}}{1.5841}} \tag{9}$$

With $\mathrm{Pr\_}D_{t\,\mathrm{e}}$ being the probability whereupon the process of expansion in a cell can take place, so that in an iteration the model simulates the growth in a sampling period.

The same procedure was applied for the inner part of the ring colonized by crabs. In this case, the function of percentage growth fitted was (ANOVA $F_{1,99} = 264.77$, $p < 0.01$, Zar, 1999):

$$\mathrm{Ci}\% = \frac{22.049}{D_{t\,\mathrm{i}}} \tag{10}$$

where $D_{t\,\mathrm{i}}$ is the internal diameter measured at time t.

When repeating the procedure to equalize the growth functions for each probability found from the model iteration, no coherent association between the dependent and independent variable was found. Therefore, it was not possible to fit a probability function in this way. However, the Ci% curve adjusted well enough to the simulated curves of high probability. If one of these curves was adopted to iterate the model, the internal diameter would lose randomness in its shape. For this reason the former shape would look very much like the arrangement of cells which would replace it. Finally, a variable probability of the following type was adopted:

$$\mathrm{Pr\_}D_{t\,\mathrm{i}} = 0.3 + 0.3\eta \tag{11}$$

where η is an uniform random number in the range [0,1]

The internal diameter vs external diameter relation (Fig. 3c), was adjusted according to the curve (ANOVA $F_{1,99} = 95.97$, $p < 0.01$, Zar, 1999):

$$D_{t\,\mathrm{i}} = 0.600 + 0.706D_{t\,\mathrm{e}} \text{ for } D_{t\,\mathrm{i}} > 0.85\ \mathrm{m} \tag{12.1}$$

$$D_{t\,\mathrm{i}} = 0D_{t\,\mathrm{e}} \text{ for } D_{t\,\mathrm{i}} \leq 0.85\ \mathrm{m} \tag{12.2}$$

So far the growth laws of internal and external diameters of plant patches were the only ones found. Still to be determined the position that the external diameters will have to adopt in the terrain when *Sarcocornia perennis* germinates and when the crabs begin to colonize the plant patches so that the measured histograms (Fig. 5a, b) can be adjusted. For an arbitrary number N of plants their position was randomly and uniformly distributed on the land surface. The diameters must fit their

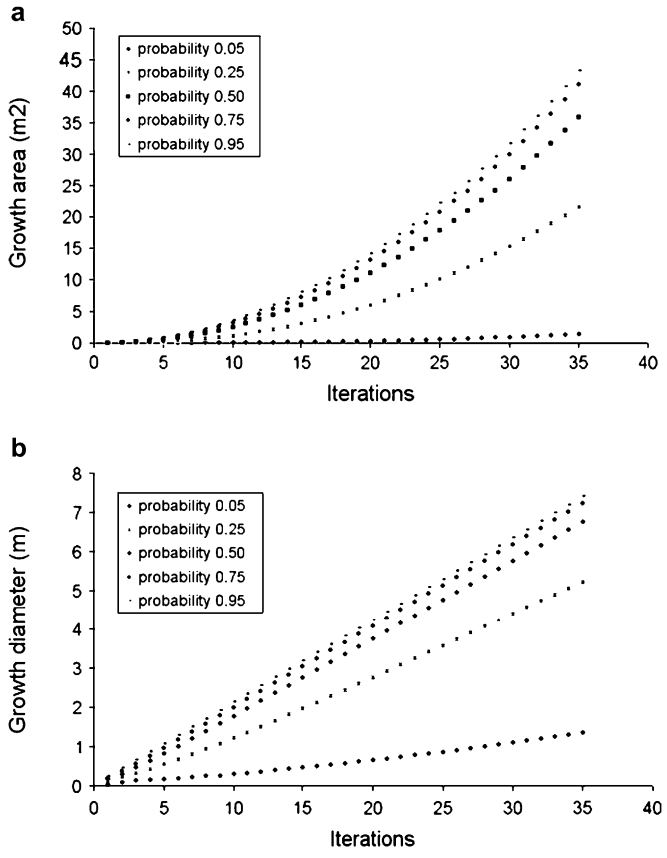

Fig. 4. (a) Simulated growth of the area of patches of *Sarcocornia perennis* for different probabilities according to the iteration number, (b) simulated growth of the diameter of patches of *S. perennis* for different probabilities according to the iteration number and (c) simulated percentage growth of the diameter of patches of *S. perennis* for different probabilities according to the iteration number.

respective histogram, that is to say, each fraction *ni* that occupies a frequency rank *i*–*n*th of classes *i* is:

$$ni = iN \tag{13}$$

The external diameter according to the iteration number is a biunivocal function. This is obtained by simulating the growth of 10 plant seeds during a larger number of iterations. Finally, the diameter was recorded as a function of the iteration number. Therefore, the percentage of seeds is known,

Table 1
Coefficients for the regression of simulations of percentage growth of external diameters of patches for different probabilities p_i. Row 7 contains the results of the Eq. (8) in correspondence with the different probabilities in row 1. * indicates highly significant regressions with F increasing

Probability (p_i)	a_i	b_i	F_{stat}	P_{stat}	Degrees freedom	D_{te}
0.01	0.4627	0.9477	42.6	<0.01	1-758	6.1958
0.02	0.4410	2.0175	331.7	<0.01	1-299	5.8923
0.03	0.6789	2.6626	608.0	<0.01	1-1267	5.2754
0.04	0.6736	3.6309	1067.0	<0.01	1-1300	4.9915
0.05	1.9640	3.7421	109.0	<0.01	1-321	3.5681
0.10	1.0196	8.2817	1313.0	<0.01	1-449	3.2483
0.15	1.2550	10.3941	3040.0	<0.01	1-541	2.5094
0.20	0.6859	13.2707	9020.0	<0.01	1-594	2.0738
0.25	0.8511	14.1703	9908.0	<0.01	1-592	1.7179
0.30	0.5326	16.0430	19170.0	<0.01	1-618	1.3000
0.35	0.5775	16.7497	36052.0	<0.01	1-619	1.0621
0.40	0.3670	17.8883	56284.0	<0.01	1-642	0.7578
0.45	0.2938	18.5397	*	*	*	0.5546
0.50	0.2164	19.1648	*	*	*	0.3507
0.55	0.3256	19.2012	*	*	*	0.3255
0.60	0.2596	19.6201	*	*	*	0.1884
0.65	0.1720	20.0671	*	*	*	0.0352
0.70	0.1974	20.1508	*	*	*	0.0054
0.75	0.1336	20.4496	*	*	*	−0.1022
0.80	0.0722	20.7373	*	*	*	−0.2106
0.85	0.0743	20.7964	*	*	*	−0.2322
0.90	0.0532	20.9009	*	*	*	−0.2729
0.95	0.0234	21.0245	*	*	*	−0.3224

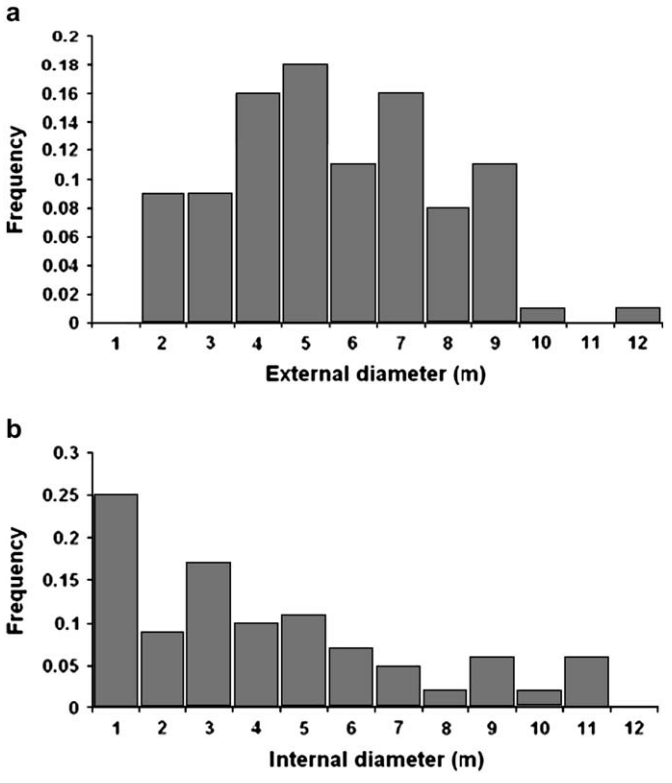

Fig. 5. Distribution histograms of diameters of patches of *Sarcocornia perennis* measured at the salt marsh. (a) External diameters and (b) internal diameters.

and also how many iterations must be made to fit the measured histogram.

When the internal diameter begins to grow according to Eq. (11) but conditioned by Eq. (12), that is to say, when $D_{t\,e}>0.85$, then, $D_{t\,i}$ does not depend on its measured real histogram. Finally, the accretion of the patches vs the external diameter was adjusted with the curve (ANOVA $F_{1,48}=53.6$, $p<0.01$, Zar, 1999):

$$h = 1.859 - 0.498 D_{t\,e} \quad (14)$$

This depression is the level value measured in the center of the ring. The patch pan formed within the ring is assumed to have a form of revolution paraboloid, whose maximum depression agrees with h in the midpoint of the ring.

2.5. Tidal creek evolution

In this step, the salt marsh is represented by the sum of the DTM topography plus the resulting topography for the plant–crab interaction. In the DTM are the typical depressions of the land that form small pans plus the ring salt pans and patch salt pans. In the following analysis, the three types of pans are considered to be only one, called pan. The next step is to find out how the pans drain when the tide is ebbing or after rains. Pans are analyzed from the point of view of their interconnection and their outflow pattern over the boundaries of the simulated field. The runoff model adopted here is not hydrodynamic since it does not consider the effect of the tidal water slope. The main process of channel growth in the studied marsh is due to the water discharge from the subbasins formed by the patch salt pans and the ring salt pans that drain the water once the tide is below the marsh level.

The delimitation of the pans is determined by analyzing the route of a drop of water placed at each grid point. We assume that the drops will move from the starting point following the path where the topographic slopes are larger. Therefore, the trajectories indicate those paths which are taken by a larger quantity of water drops, and those which are more likely to be eroded. All the water drops that drift to a common point will share the same pan. Analysis of these pans in the whole matrix results in a drainage basin map of the DTM.

The interconnection of these pans will define resultant basins where the tidal creek will grow. Each pan drains off from the Lowest Basin Border Point (LBBP) towards its adjacent pan and this in turn from its LBBP towards another neighbour pan. The LBBP, as its name indicates, is the point along the pan border having the absolute minimum elevation. When two adjacent pans have opposite exit points, they turn into an endorreic pan (without water outflow). In this case, two pans are taken as only one and the analysis continues until the basin drains from the border of the matrix.

We assume that the amount of water that drains from each pan is proportional to its area. Each pan that receives water keeps the information on the quantity of accumulated water that brings its tributary pans. Thus, the amount of water that overflows the matrix and flows outwards is known. Finally, for each basin, the creek grows following the pans which contribute the larger flows. The creek starts in a pan at the edge of the matrix and grows towards the interior of the matrix.

The path that the channels follow is obtained in the following way:

- By connecting the points where the pans overflow with those of minimum level.
- Then from these points towards the point where the tributary pan overflows.
- This procedure is applied to all pans in the DTM and the creek follows the path that is crossed by the largest quantity of water drops.
- Secondary creeks in each basin are not considered in the analysis.

3. Results and model verification

One simulation was made on a rectangular matrix of 1240 cells (10 cm cell^{-1}) for the DTM. Two simulations were made for the plant–crab interaction on a rectangular matrix of 2480 cells (5 cm cell^{-1}) plus the DTM. The simulated area is square of 124 m on the side for all cases. In the two plant–crab interaction simulations the model generated 343 patches. The distribution histograms of the obtained external diameters (Fig. 7a, c) were compared with the real data (Fig. 5a) by a test of goodness of fit $\chi 2$ (Montgomery and Runger, 1996). Since the number of external original diameters measured (d_{eo}) was lower than the amount of simulated diameters (d_{es}), the sample was normalized by dividing the frequency of the latter by the factor d_{es}/d_{eo} to be able to make the test. In all the cases, the simulated distribution is similar to the original distribution (Table 2).

Furthermore, the relation between internal vs external diameter remains inside the cloud of points of the original information and they are distributed evenly on both sides of the regression line (Fig. 6). With a Student t-test (Zar, 1999) we compared the line slope of d_i vs d_e in the series of simulated and real data. In the both cases the straight line slopes were statistically similar to the original data (Table 3).

However, the histograms of distribution of simulated internal diameters (Fig. 7b, d) show differences with respect to the measured histogram. This is because they are generated by Eq. (12), which cannot reproduce the variance of the original

Table 2
Results of for the test of goodness of fit of the histograms of external and internal diameters, respectively. The histograms of the external simulated diameters fitted well to the real measured histogram, while the histograms of the internal diameters did not fit well to the real measured histogram

	Sim 1	Sim 2
df	9	9
χ^2-d_e	2.53	2.04
α-d_e	0.975	0.975
χ^2-critic d_e	2.7	2.7
χ^2-d_i	61.41	57.24
α-d_i	0.05	0.05
χ^2-critic d_i	2.7	2.7

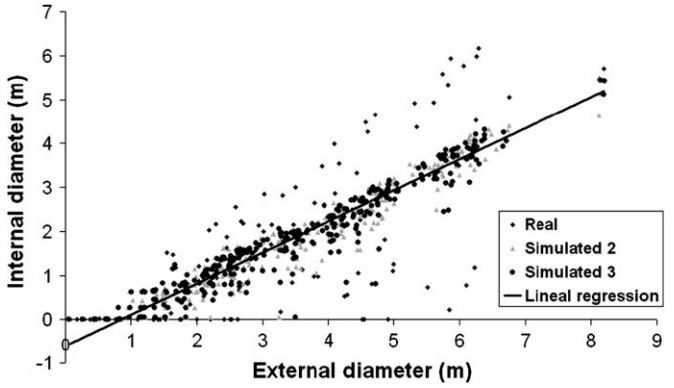

Fig. 6. Real and simulated relation between the internal diameters and external diameters. The straight line is the regression of the real data.

sample. A test of goodness of fit was performed to establish whether the simulated histogram fits the real one, but in both cases there was no significant statistical evidence to accept the hypothesis (Table 2). Nevertheless, a test of comparison of means concluded that the averages of the real and simulated internal patches are equal (ANOVA $F_{2,783} = 0.094$, $p > 0.91$, Zar, 1999)

In order to compare the shape of a real plant patch with the simulated patches, we compared their fractal dimension. A total of 27 plant patches was obtained from aerial photographs (Fig. 1b) and another 27 were chosen randomly from the model applying the relation (Hastings and Sugiahra, 1993; Turner, 1989):

$$P = KA^{D/2} \tag{15}$$

where P is the perimeter of the patch, K is a proportionality constant, A is the patch area and D is the fractal dimension of P.

For the regression with the original data, we found that $K = 4.850$ and $D = 0.943$ (ANOVA $F_{1,25} = 282.8$, $p < 0.01$, Zar, 1999) whereas for the regression of patches generated by the model we estimated that $K = 2.912$ and $D = 1.088$ (ANOVA $F_{1,25} = 1764.9$, $p < 0.01$, Zar, 1999). For both regressions the tendencies were similar; however, the interval of confidence of the simulated patches was within the interval of confidence of the real patches (Fig. 8), which may indicate that the dispersion of the real data does not allow us to find significant differences between both regressions.

The DTM was generated for a region coincident with the dimensions of the area where the patches of plants were simulated. The application of a lowpass filter allowed the adaption of the original model generated by the fractal algorithm to the characteristic of the salt marsh. Then we added the effects of two simulations of the terrain for plants and crabs. Therefore, we had three land situations, one with the DTM without biological disturbances (case 1, Fig. 9a) and two with the DTM including these disturbances (cases 2 and 3, Fig. 9d, g).

Finally, the resulting salt pans for the three land situations were analyzed. For case 1 (control) 205 pans were obtained, whereas for cases 2 and 3, 726 and 744 pans were obtained, respectively. The basins were different for the three modeled situations (Fig. 9b, e, h). Also the trajectories of the tidal creeks were totally altered by the additional effect of the plants with crabs in the salt marsh (Fig. 9c, f, i). The tidal creeks deviated from their trajectories towards these patch-pans. In some cases, tidal creeks different from the original ones were generated by a combination of trajectories, whereas in other cases new creeks were generated unaffected by the original topography.

Table 3
Results of the comparison of the real and simulated straight lines of regression between external and internal diameters. Both simulated relations turned out to be equal to the real relation measured in the salt marsh

	Sim 1	Sim 2
t	0.644	0.261
df	439	439
α	0.1	0.1
t-critic	1.2	1.2

4. Discussion and conclusions

The Cellular Automata model proves to be adequate in reproducing the interaction effects between plants and crabs in the salt marsh. The histogram of external diameters, the relations between diameters and the power law correlation between the area and the perimeter were statistically identical to the measured data. However, the histogram of internal diameters was not reproduced satisfactorily; although the model has been able to reproduce its mean and variance. Nevertheless, the internal diameter only has a landscape importance, because it does not become involved in the modification of the topography, since the depression and shape of the patches are a function of the external diameter.

Although most of the flow associated with tidal channels and coastal wetlands is driven by the energy slope induced by the tide, as it occurs in our marsh when it is inundated, most of the erosion and stream retreat observed in the study site is produced by the continuous discharge of water accumulated on the pans either as retained from a previous tidal event or from rainfall. As this marsh is only covered by the tides about 40 times a year, rainfall and even some groundwater outflow through the crab burrows concentrated in the pans play the main role in shaping the streams by simply gravitational circulation.

The water drainage study of the basins showed that this interaction does indeed modify the development of tidal creeks. Creeks were attracted towards the pans generated by the crabs (Fig. 9c, f, i). The resultant basins modified their shape and increased their area of contribution due to the presence of the ring salt pans and patch salt pans. In the simulations with vegetation, the disturbance in the topography generated tidal creeks totally unrelated from those generated in the original marsh. These mechanisms control the spatial and temporary growth dynamics of the tidal creeks. Spatially, they form the path where the channel will develop, and temporally, we

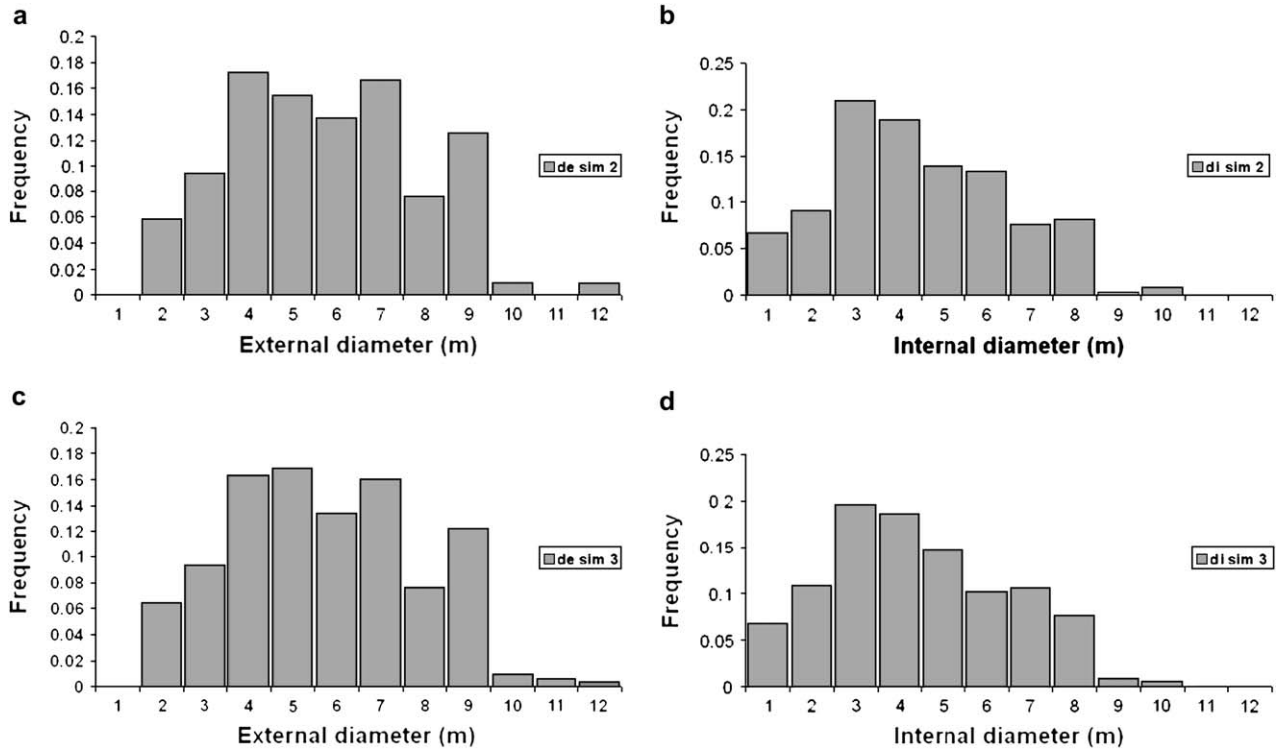

Fig. 7. (a) Histogram of the simulated external diameters of *Sarcocornia perennis* and (b) histogram of the simulated internal diameters of *S. perennis*.

observed that the mean retreat length rate is proportional to its drainage subbasin. These factors exert a greater influence than the water surface gradient, which has seen that dominates in the intertidal ambient (Rinaldo et al., 1999a,b; Fagherazzi and Sun, 2004).

The model was thought only to reproduce the effects of the interaction between the plants and the crabs in the topography in the present state of the salt marsh. The model is not biologically complete because we did not contemplate the natality and mortality rates of the patches of plants and crabs. The landscape and the bioturbation are reproduced correctly in the last iterations because it is the point where the conditions measured in the land are fulfilled. However, the early stages of the model not necessarily reflect what actually happened in the marsh as we lack the adequate data to compare. Furthermore, maintaining the model running forward will result in a salt marsh completely covered by plants and crabs due to the lack of the natality and mortality controls.

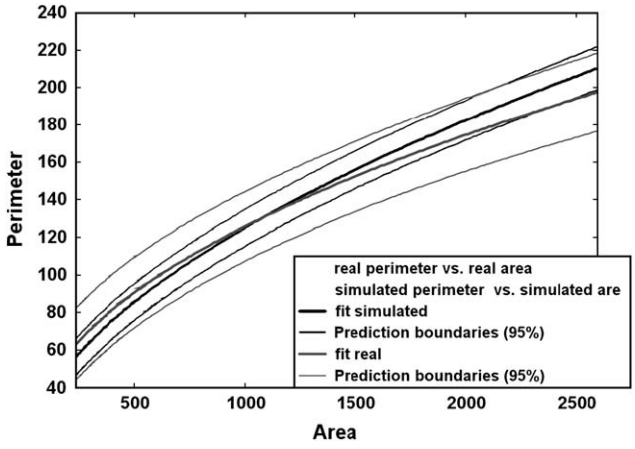

Fig. 8. Relations between area and perimeter of the patches of *Sarcocornia perennis* simulated and real. Units are in cells. The interval of confidence of the simulated patches is inside the interval of confidence of the real patches.

These laws can be easily added and the model could then provide extended information about how the system behaves under different events on the salt marsh (Wiegand pers. com.). Also, if the natality or mortality of only one species is known, it is possible to deduce the mortality or natality rates of the other in order to balance the system. In the present case, we did not include the seasonal variability of these processes either. The modeled processes occur in the warm period for the Southern Hemisphere, mainly from December to March. In order to reach the present state, the model made 182 iterations, which means a time interval of 45 years. Field data were gathered in the period 2001–2003. Actually the patches were discovered in 2001, so there is no previous information of status of the salt marsh to calibrate the model in its first iterations. Therefore, the simulation coincides with the current state of the marsh and does not determine what occurred before.

At this stage it is not possible to quantify the erosion produced by the mechanism of creek formation promoted by the biological interaction. Nevertheless, it is possible to make an adaptation to quantify how much sediment has been removed due to the depression effect that occurs at the patches in the whole marsh in order to make a short term prediction. Finally, the methodology developed has proved to be an excellent tool

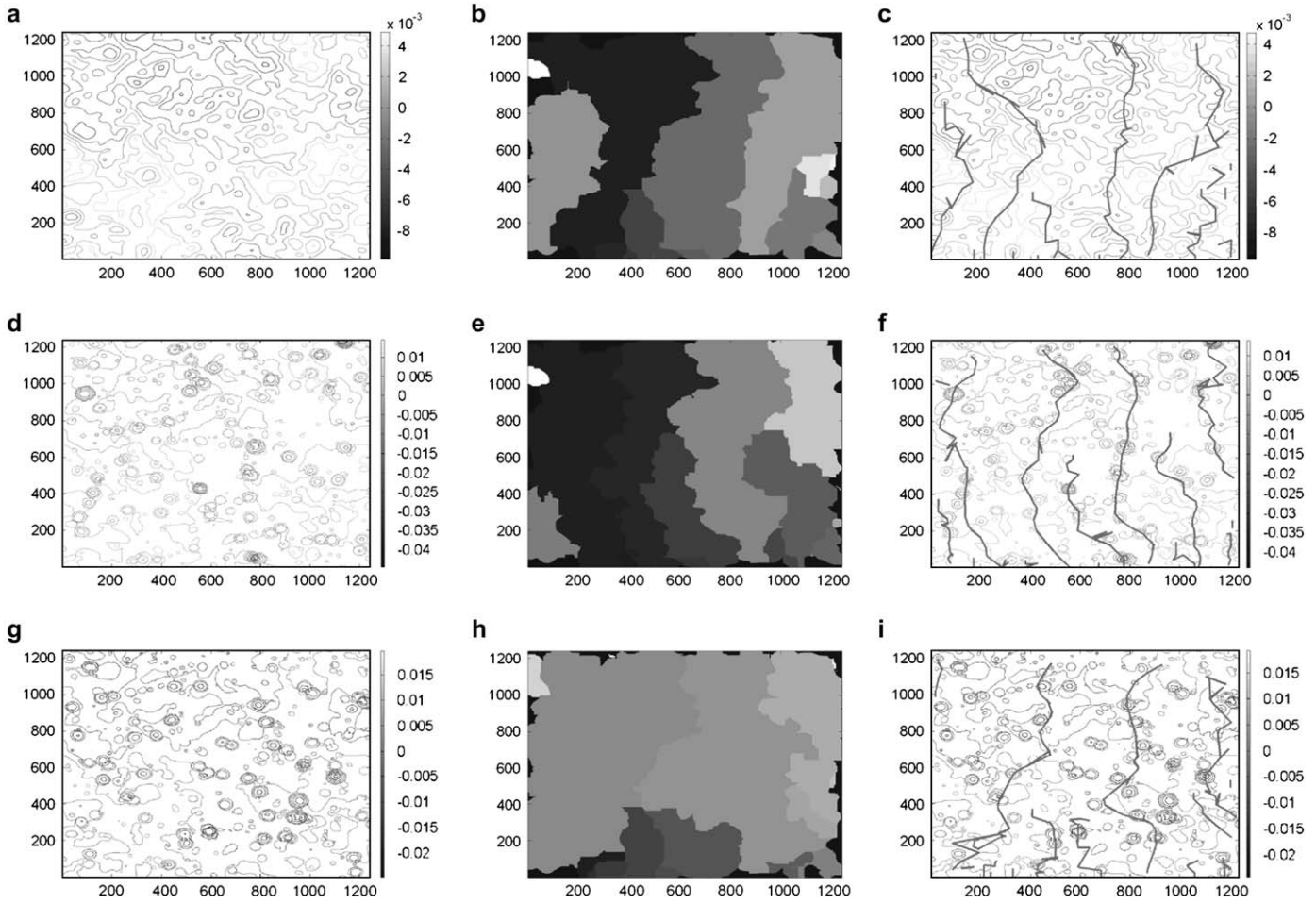

Fig. 9. Level curves of the digital terrain model: (a) simulation 1: digital terrain model without added disturbances. (d) Simulation 2: terrain resulting of simulation 1 plus the accretion of the patches of the simulation 2. (g) Simulation 2: terrain resulting from simulation 1 plus the accretion of the patches of the simulation 3. Resultant drainage basins of the DTM: (b) simulation 1: drainage basins of the DTM without added disturbances. (e) Simulation 2: drainage basins of the terrain resulting from simulation 1 plus the accretion of the patches of the simulation 2. (h) Simulation 3: drainage basins of the terrain resulting from simulation 1 plus the accretion of the patches of the simulation 3. Resulting paths of simulated tidal creeks. (c) Simulation 1: paths of simulated tidal creeks without added disturbances. (f) Simulation 2: paths of simulated tidal creeks resulting from simulation 1 plus the accretion of the patches of the simulation 2. (i) Simulation 3: patches of simulated tidal creeks resulting from simulation 1 plus the accretion of the patches of simulation 3.

for patch growth simulation. The model dynamics can be adapted to different laws (i.e. processes), which would provide a different formula for the probability of patch dilation. The shape can be obtained changing the dilative pattern.

References

Aassine, S., El Jai, M.C., 2002. Vegetation dynamics modelling: a method for coupling local and space dynamics. Ecological Modelling 154, 237–249.

Bandini, S., Pavesi, G., 2002. Simulation of vegetable populations dynamics based on cellular automata. In: Bandini, S., Chopard, B., Tomassini, M. (Eds.), Proceedings of Fifth International Conference on Cellular Automata for Research and Industry (ACRI 2002). Lecture Notes in Computer Science, 202–209 (Springer-Verlag, Berlin).

Bortolus, A., Iribarne, O., 1999. Effects of the SW Atlantic burrowing crab *Chasmagnathus granulata* on a *Spartina* salt marsh. Marine Ecology Progress Series 178, 78–88.

Botto, F., Iribarne, O., 1999. Effect of the burrowing crab Chasmagnathus granulata on the benthic community of a SW Atlantic coastal lagoon. Journal of Experimental Marine Biology and Ecology 241, 263–284.

Botto, F., Iribarne, O., 2000. Contrasting effects of two burrowing crabs (*Chasmagnathus granulata* and *Uca uruguayensis*) on sediment composition and transport in estuarine environments. Estuarine, Coastal and Shelf Science 51, 141–151.

Chapman, V.J., 1960. Salt Marshes and Salt Deserts of the World. Leonard Hill, London.

D'Ambrosio, D., Di Gregorio, S., Gabriele, S., Gaudio, R., 2001. A cellular automata model for erosion by water. Physics and Chemistry of the Earth (B) 26 (1), 33–39.

Dunkerley, D.L., 1997. Banded vegetation: survival under drought and grazing pressure based on a simple cellular automaton model. Journal of Arid Environments 35, 419–428.

El Yacoubi, S., El Jai, A., Jacewicz, P., Pausas, J.G., 2003. LUCAS: an original tool for landscape modelling. Environmental Modelling and Software 18, 429–437.

Fagherazzi, S., Sun, T., 2004. A stochastic model for the formation of channel networks in tidal marshes. Geophysical Research Letters 31 (21), L21503. doi:10.1029/2004GL020965.

Fagherazzi, S., Bortoluzzi, A., Dietrich, W.E., Adami, A., Lanzoni, S., Marani, M., Rinaldo, A., 1999. Tidal networks, 1, automatic network extraction and preliminary scaling features from digital terrain maps. Water Resources Research 35 (12), 3891–3904.

Fournier, A., Fussel, D., Carpenter, L., 1982. Computer rendering of stochastic models. Communications of the ACM 25, 371–384.

Frey, R.W., Basan, P.B., 1985. Coastal salt marshes. In: Davis, R.A. (Ed.), Coastal Sedimentary Environments. Springer Verlag, New York, pp. 187–224.

Garofalo, D., 1980. The influence of wetland vegetation on tidal stream channel migration and morphology. Estuaries 3, 258–270.

González, R.C., Woods, R.E., 1992. Digital Image Processing. Addison-Wesley.

Haralick, R.M., Shapiro, L.G., 1992. Computer and Robot Vision, vol. I. Addison-Wesley.

Hastings, H.M., Sugiahra, G., 1993. Fractals: A User's Guide for the Natural Sciences. Oxford University Press.

Howard, A.D., Dietrich, W.E., Seidl, M.A., 1994. Modeling Alluvial erosion on regional to continental scales. Journal of Geophysical Research 99, 1386–1397.

Iribarne, O., Bortolus, A., Botto, F., 1997. Between habitat differences in burrow characteristics and trophic modes in the south western Atlantic burrowing crab *Chasmagnathus granulata*. Marine Ecology Progress Series 155, 137–145.

Kelley, A.D., Malin, M.C., Nielson, G.M., 1988. Terrain simulation using a model of stream erosion. Computer Graphics 22 (4), 263–268.

Mandelbrot, B., 1982. The Fractal Geometry of Nature. W.H. Freeman, San Francisco.

Marani, M., Lanzoni, S., Zandolin, D., Seminara, G., Rinaldo, A., 2002. Tidal meanders. Water Resources Research 38 (11), 1225. doi:10.1029/2001WR000404.

Mastin, G.A., Wattererg, P.A., Mareda, J.F., 1987. Fourier synthesis of ocean waves. IEEE Computer Graphics and Applications 7 (3), 16–23.

Matsinos, Y.G., Troumbis, A.Y., 2002. Modeling competition, dispersal and effects of disturbance in the dynamics of a grassland community using a cellular automaton model. Ecological Modelling 149, 71–83.

Miller, G.S.P., 1986. The definition and rendering of terrain maps. Computer Graphics 20 (4), 39–48.

Montgomery, D.C., Runger, G.C., 1996. Probabilidad y Estadística Aplicadas a la Ingeniería. McGraw-Hill.

Muagrave, F.K., Kolb, C.E., Mace, R.S., 1989. The synthesis and rendering of eroded fractal terrains. Computer Graphics 23 (3), 41–48.

Perillo, G.M.E., Codignotto, J.O., 1989. Ambientes costeros. Boletín Sedimentológico 4, 137–159.

Perillo, G.M.E., Iribarne, O.O., 2003a. Process of tidal channel development in salt marshes and freshwater. Earth Surface Processes and Landforms 28, 1473–1482.

Perillo, G.M.E., Iribarne, O.O., 2003b. New mechanism studied for creek formation in tidal flats: from crabs to tidal channels. Eos Transaction, American Geophysical Union 84, 1–5.

Pestrong, R., 1965. The development of drainage patterns on tidal marshes. Stanford University Publication in Geological Science, Technical Report 10. Stanford University, Stanford, California.

Pestrong, R., 1972. Tidal flat sedimentation at Cooley Landing, southwest San Francisco Bay. Sedimentary Geology 8, 251–288.

Pethick, J.S., 1980. Velocity surges and asymmetry in tidal channels. Estuarine and Coastal Marine Science 11, 331–345.

Piccolo, M.C., Perillo, G.M.E., 1999. Estuaries of Argentina: a review. In: Perillo, G.M.E., Piccolo, M.C., Pino Quivira, M. (Eds.), Estuaries of South America: Their Geomorphology and Dynamics. Environmental Science Series. Springer Verlag, Berlín, pp. 101–132.

Rinaldo, A., Fagherazzi, S., Lanzoni, S., Marani, M., Dietrich, W.E., 1999a. Tidal networks, 2, Watershed delineation and comparative network morphology. Water Resources Research 35 (12), 3905–3917.

Rinaldo, A., Fagherazzi, S., Lanzoni, S., Marani, M., Dietrich, W.E., 1999b. Tidal networks, 3, Landscape-forming discharges and studies in empirical geomorphic relationships. Water Resources Research 35 (12), 3919–3929.

Saupe, D., 1988. Algorithms for random fractals. In: Peitgen, H.O., Saupe, D. (Eds.), The Science of Fractal Images. Springer-Verlag, New York, pp. 71–136.

Sipper, M., 1997. Evolution of parallel cellular machines: the cellular programming approach. Lecture Notes in Computer Science 1194 (Springer, Berlin).

Smith, T.R., Birnir, B., Merchant, G.E., 1997. Towards an elementary theory of drainage basin evolution. I. The theoretical basis. Computers and Geosciences 23, 811–822.

Spivak, E., Anger, K., Luppi, T., Bas, C., Ismael, D., 1994. Distribution and habitat preferences of two grapsid crab species in Mar Chiquita Lagoon (province of Buenos Aires, Argentina). Helgolander Meeresuntersuchungen 48, 59–78.

Turner, M.G., 1989. Landscape ecology: the effect of pattern on process. Annual Review of Ecology and Systematics 20, 171–197.

Voss, R.F., 1985. Random fractal forgeries. In: Earnshaw, R.A. (Ed.), Fundamental Algorithms for Computer Graphics. Springer Verlag, Berlin, pp. 39–48.

Wei luo, 2001. LANDSAP: a coupled surface and subsurface cellular automata model for landform simulation. Computer Geosciences 27, 363–367.

Wolfram, S., 1984. Universality and complexity in cellular automata. Physica 10D, 1–35.

Wolfram, S., 1994. Cellular Automata and Complexity. Addison-Wesley Publishing Company (Science Mathematics Computing).

Worsch, T., 1999. Simulation of cellular automata. Future Generation Computer Systems 16, 157–170.

Zar, J.H., 1999. Biostatistical Analysis. Prentice-Hall, Inc., Englewood Cliffs, New Jersey, USA.